JOURNAL OF VIROLOGY, Jan. 2008, p. 451–460 Vol. 82, No. 1
0022-538X/08/$08.00+0 doi:10.1128/JVI.01251-07

Intracellular Restriction of a Productive Noncytopathic Coronavirus Infection▽

Olga Slobodskaya, Alexander Laarman,# and Willy J. M. Spaan*

Molecular Virology Laboratory, Department of Medical Microbiology, Center of Infectious Diseases, Leiden University Medical Center, P.O. Box 9600, 2300 RC Leiden, The Netherlands

Received 8 June 2007/Accepted 13 October 2007

Virus infection in vitro can either result in a cytopathic effect (CPE) or proceed without visible changes in infected cells (noncytopathic infection). We are interested in understanding the mechanisms controlling the impact of coronavirus infection on host cells. To this end, we compared a productive, noncytopathic infection of murine hepatitis virus (MHV) strain A59 in the fibroblastlike cell line NIH 3T3 with cytopathic MHV infections. Infected NIH 3T3 cells could be cultured for up to 4 weeks without apparent CPE and yet produce virus at 10^7 to 10^8 PFU/ml. Using flow cytometry, we demonstrated that NIH 3T3 cells expressed as much MHV receptor CEACAM1 as other cell lines which die from MHV infection. In contrast, using quantitative reverse transcription-PCR and metabolic labeling of RNA, we found that the rate of viral RNA amplification in NIH 3T3 cells was lower than the rate in cells in which MHV induces a CPE. The rate of cellular RNA synthesis in contact-inhibited confluent NIH 3T3 cells was also lower than in cells permissive to cytopathic MHV infection. However, the induction of cellular RNA synthesis in growing NIH 3T3 cells did not result in an increase of either viral RNA amplification or CPE. Our results suggest that a specific, receptor CEACAM1-independent mechanism restricting coronaviral RNA synthesis and CPE is present in NIH 3T3 and, possibly, other cells with preserved contact inhibition.

Coronaviruses belong to the *Coronaviridae* family in the *Nidovirales* order. Coronavirus infections can follow different scenarios in vivo, as well as in vitro, suggesting complex and diverse interaction with their hosts. Viral genome expression and molecular mechanisms of virus-host interaction have mostly been studied in the context of efficient coronavirus replication in a lytic infection of cultured, transformed cells. Cytopathic infection with one of the best-studied coronaviruses, murine hepatitis virus (MHV), causes drastic changes in the cellular infrastructure (20, 36) and metabolism (14, 37, 44) and results in cell death. Coronavirus infection in vitro can take a different course and exhibit limited or no cytopathic effect (CPE) or virus-induced cell death. Productive noncytopathic infections have been described for primary cells or relatively differentiated cell lines infected with coronaviruses MHV (19, 21, 27), human coronavirus OC43 (1), human coronavirus 229E (2), and severe acute respiratory syndrome (SARS) coronavirus (5). Sturman and Takemoto reported that MHV infection of the mouse BALB/3T3 cell line produced high yields of virus but showed little CPE within 1 day postinfection (p.i.) (40). Mouse embryo fibroblast BALB/3T3 cell lines are obtained in such a way that the cells exhibit the contact inhibition that is characteristic of nontransformed cells in vivo (41). The coronavirus CPE became pronounced when BALB/3T3 cells were transformed, either spontaneously or by infection with oncogenic viruses (40). Which mechanisms or host factors prevent CPE and virus-induced cell death in nontransformed cells remains unknown.

The best-studied host factor participating in coronavirus infection is the coronavirus receptor which determines the coronavirus host range. The exogenous expression of a receptor in cells originally resistant to infection renders the cells susceptible to the respective coronavirus (10, 23, 43). The easy switch of host specificity by providing a proper receptor suggests that other host factors required for coronavirus replication are present in many cells. However, not all cells expressing the appropriate receptor can be efficiently infected by a coronavirus. SARS coronavirus did not replicate in human colorectal adenocarcinoma cell lines LS-180 and SW620, which expressed the SARS coronavirus receptor ACE2 in higher quantities than the susceptible cell line LoVo (5). Mature and immature dendritic cells expressing similar amounts of the MHV receptor CEACAM1 were infected by MHV with different efficiencies, immature dendritic cells being much more resistant (48). Besides mediating virus entry, MHV receptor CEACAM1 plays a role in the CPE development by promoting cell-to-cell fusion. In addition, the accumulation of the intracellular complexes of the receptor with the MHV spike glycoprotein were shown to be cytotoxic (29).

The postentry steps of coronavirus replication start with the translation of the 27- to 32-kb-long genome RNA (gRNA). Two large, overlapping open reading frames (ORFs) occupying two-thirds of the coronavirus genome encode two polyproteins which are processed by viral proteinases into 14 to 16 nonstructural proteins. The majority of these proteins have predicted or proven functions in viral RNA synthesis (see reference 33). Viral RNA synthesis proceeds by the replication of gRNA and the transcription of a 3′-coterminally nested set

* Corresponding author. Mailing address: Molecular Virology Laboratory, Department of Medical Microbiology, Leiden University Medical Center, LUMC E4-P, P.O. Box 9600, 2300 RC Leiden, The Netherlands. Phone: 31715261652. Fax: 31715261667. E-mail: w.j.m.spaan@lumc.nl.

Present address: Medical Microbiology, University Medical Center Utrecht, Heidelberglaan 100, 3584 CX Utrecht, The Netherlands.

▽ Published ahead of print on 24 October 2007.

of subgenomic RNAs (sgRNAs). These sgRNAs are translated into accessory proteins and proteins that constitute virus particles. Currently, not much is known about host factors that participate in the intracellular steps of virus replication (see references 11 and 18). The ubiquitin-proteasome system was shown to facilitate MHV strain JHM infection, but not strain A59 (MHV-A59) infection (46). Several cellular proteins, like hnRNP A1, (22), PTB (15), SYNCRYP (8), mitochondrial aconitase (25), and poly(A)-binding protein (39), have been shown to bind to coronavirus RNA. Modulation of the expression levels or expression of mutant hnRNP A1, PTB, and SYNCRYP affected viral RNA replication, indicating that these host factors are required for efficient viral RNA synthesis (7, 8, 35).

We are interested in understanding the mechanism that controls the impact of coronavirus infection on host cells. This study compared a productive noncytopathic infection of MHV-A59 in the NIH 3T3 cell line with cytopathic infections of the same virus in several other murine cell lines. We found that noncytopathic infection was accompanied by reduced amplification of viral RNA. Our results suggest that a host factor present in NIH 3T3 cells and, possibly, other cells with preserved contact inhibition restricts coronaviral RNA abundance and, consequently, the CPE.

MATERIALS AND METHODS

Cells and viruses. Mouse fibroblastlike NIH 3T3, L929, and myoblast C2C12 cells were obtained from the American Type Culture Collection (ATCC) (ATCC numbers CRL-1658, CCL-1, and CRL-1772, respectively). Mouse fibroblastlike 17Cl 1, L, Sac(-), and astrocytoma DBT cells were obtained from P. Rottier's laboratory in Utrecht, the Netherlands. All cell lines were grown with Dulbecco modified Eagle medium (DMEM) supplemented with 100 units/ml of penicillin, 100 μg/ml of streptomycin, and 8% fetal calf serum (FCS). After infection, cells were incubated in the same medium with the same antibiotics but with 3% FCS. Cells were passaged every 3 days, the NIH 3T3 cells by the transfer of 3×10^5 cells into a new 75-cm^2 flask and the other cell lines by being split at ratios of 1:10 to 1:30. MHV-A59 was obtained from the ATCC (38). MHV-GFP (green fluorescent protein) (originally named $S_{A59}R_{EGFP}$ by the authors) (31), a recombinant MHV-A59 virus which encodes GFP in sgRNA4, was a kind gift from S. Weiss.

Virus titration and infectious center assay. Viral titers were determined in PFU/ml on L cells and in 50% tissue culture infectious dose per ml ($TCID_{50}$/ml) on L, NIH 3T3, and DBT cells. In the $TCID_{50}$ assay, wells with infected cells were scored at day 3 p.i. L and DBT cells were scored for CPE. Productive infection of NIH 3T3 cells was detected by inoculating the medium on L cells. The $TCID_{50}$ was calculated by the method of Reed and Muench (29a). The infectious center assay was done as described previously (24).

Viral infection and RNA isolation. Subconfluent monolayers of L, DBT, and NIH 3T3 cells, seeded the day before, were washed once with phosphate-buffered saline (PBS) and inoculated with MHV-A59 in DMEM–3% FCS. After 1 h at 37°C, the inoculum was removed, the cells were washed twice with PBS, DMEM with 3% FCS was added, and the cells were incubated at 37°C. At the indicated time points, the medium was collected to determine virus titers and total RNA was isolated from the monolayer by using TRIzol reagent (Gibco BRL) as recommended by the manufacturer. The RNA concentration was determined spectrophotometrically.

INT mRNA and viral RNA analysis. Quantitative reverse transcription-PCR (RT-qPCR) was performed as described previously (44) with the addition of DNase I treatment of the RNA prior to the reverse transcription. One set of primers specific for the MHV-A59 3′ untranslated region was used for the detection of total viral RNA (g+sgRNA). Another set, specific for a locus in MHV-A59 *orf1b*, was used for the detection of gRNA only. On the basis of the RT-qPCR results, the rate of viral gRNA amplification was calculated as the cube root of the ratio of the gRNA amount at 6 and 3 h p.i. It reflected the number of molecules that one molecule yields in 1 h. The induction of immediate-early interferons (INT) was examined with primers specific for the mRNA of INTα4 and INTβ (44). For Northern analysis of viral RNA, 4 μg of total cellular RNA was separated in a 1% denaturing agarose gel containing 1.1 M formaldehyde, 10 mM MOPS, 5 mM sodium acetate, and 1 mM EDTA, pH 7.5. Viral RNA was detected by in-gel hybridization with a ^{32}P-labeled oligonucleotide complementary to nucleotides 31226 to 31245 of the MHV-A59 genome. Bound radioactivity was detected by using phosphoimager technology (Molecular Imager; Bio-Rad).

Metabolic labeling. For viral RNA labeling, cells were MHV or mock infected as described above. At 1 h p.i., 1 μg/ml actinomycin D was added to the medium, followed by the addition of [^{3}H]uridine (Amersham) at a concentration of 50 μCi/ml at 3, 5, 7, and 9 h p.i. For cellular RNA and protein labeling, NIH 3T3 cells were incubated in the presence of either [^{3}H]uridine (20 μCi/ml) or ^{35}S-ProMix (50 μCi/ml; Amersham). After 1 h of incubation with a radioactive label, the cells were lysed in PBS containing 1% Triton X-100, 1% sodium dodecyl sulfate. Labeling was performed in duplicate, and the amount of acid-insoluble radioactivity was determined by scintillation counting.

Cell death assay. Cell death was determined by measuring the activity of adenylate kinase (AK) released from dying cells into the culture medium by using a ToxiLight BioAssay (Cambrex) according to the manufacturer's protocol. The FCS that was used to supplement the culture medium in this assay was incubated for 15 min at 56°C in order to reduce background AK activity. The AK activity, measured in relative units, was corrected for the background level and normalized to 10^3 cells.

Flow cytometry. Cells infected with MHV-GFP were trypsinized at 6 and 12 h p.i., fixed in PBS with 3% paraformaldehyde, and analyzed by flow cytometry. For CEACAM1 staining, cells were seeded as for an infection experiment. The next day, cells were harvested by mild trypsinization and 10^5 cells were incubated with CC1 monoclonal antibody to CEACAM1 (kindly provided by K. Holmes) and subsequently with the second goat anti-mouse immunoglobulin G antibody conjugated with fluorescein isothiocyanate. An autofluorescence control was prepared by omitting the first antibody from the incubation. The fluorescence intensity of the 10^4 to 2×10^4 cells was analyzed by using a FACSCalibur (Becton Dickinson) and CellQuest Pro software. The proportion of cells expressing CEACAM1 was determined by subtracting the histogram of the control from that of CEACAM1-stained cells and calculating the ratio of the resulting cell number and the total number of analyzed cells. The relative density of the receptor on the cell surface was calculated as a ratio of the mean fluorescence intensity of CEACAM1-positive cells and the autofluorescence control. Staining and analysis were repeated at least twice for each cell line, with two replicates in each experiment, and the means and standard deviations of the results were calculated.

RESULTS

Productive noncytopathic MHV infection in NIH 3T3 cells. For our study of host cell-virus interactions that control cytopathicity, we selected MHV-A59 and the continuous fibroblastlike NIH 3T3 cell line, following a previous report of a noncytopathic infection of MHV in 3T3 cells (40). No CPE or cell death were detected in the NIH 3T3 cells within the first 24 h of infection. (Fig. 1A). At days 2 to 4 p.i., small syncytia could be observed within the monolayer. The density of the infected cell culture, however, was similar to that of the mock-infected control. Next, we infected NIH 3T3 or L cells, in which MHV causes a rapid CPE (Fig. 1A), with a range of viral doses (0.01 to 100 PFU per cell) and determined virus titers in the first 24 h. Despite the contrasting fates of the two infected cell lines, the kinetics of virus production were similar for all doses tested (Fig. 1A, B). Infection of NIH 3T3 cells developed into a productive, persistent infection without noticeable cell death. The infected cells constantly produced high titers of virus (10^7 to 10^8 PFU/ml) and could be maintained for at least 1 month without splitting (Fig. 1C). In the mock- and MHV-infected NIH 3T3 cell cultures, a number of cells were dying and detaching from the surface, but both monolayers maintained similar densities throughout the observation period of 1 month.

To gain insight into the mechanism that controls the infec-

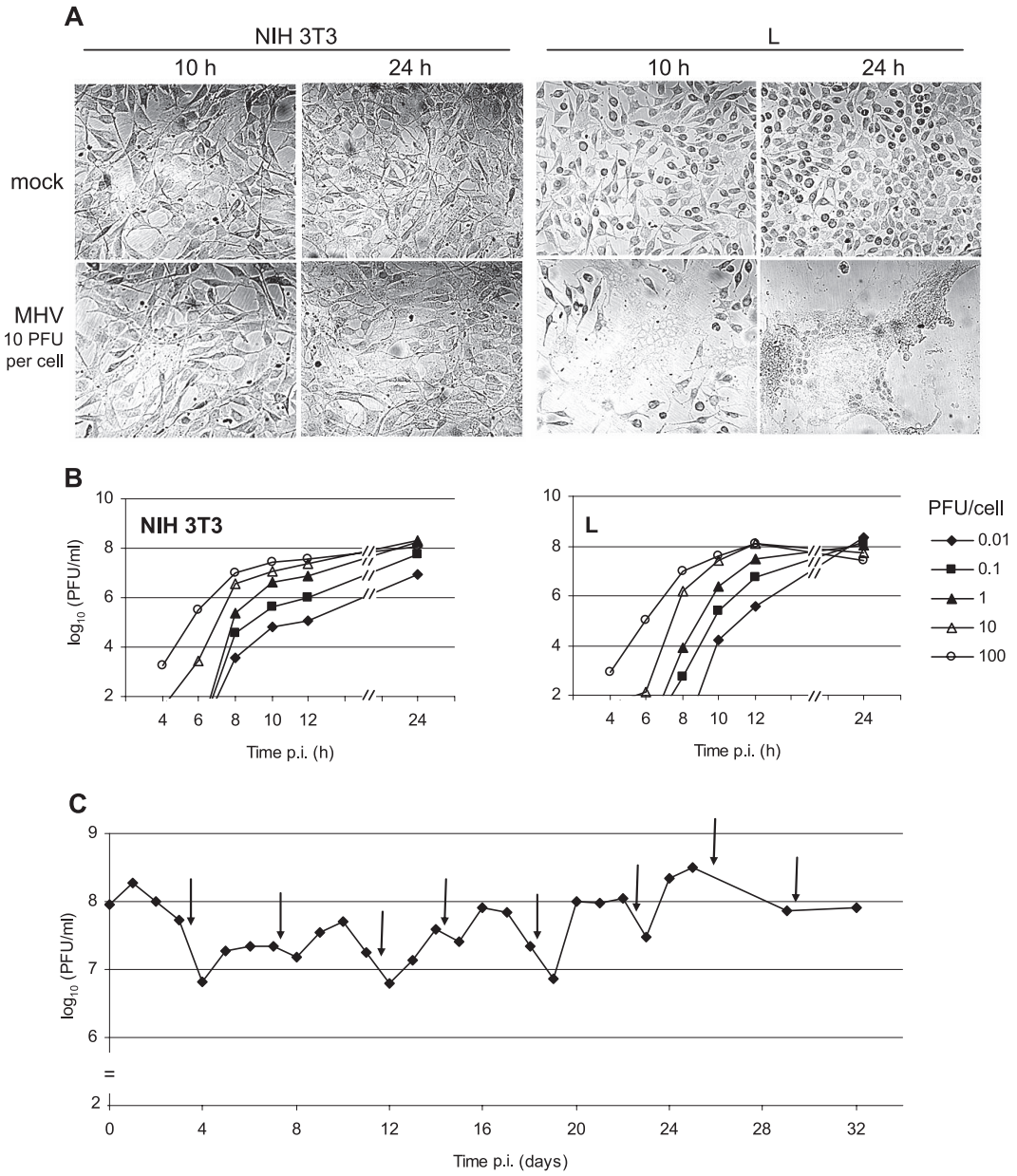

FIG. 1. Appearance of the monolayers and MHV-A59 yields in NIH 3T3 and L cells. (A) Appearance and densities of mock- and MHV-infected cells (magnification, ×70). Infection in L cells resulted in the formation of large syncytia (10 h p.i.), with complete destruction of the monolayer at 24 h p.i. (B) At 4, 5, 6, 8, 10, 12, and 24 h p.i., the incubation media of NIH 3T3 and L cells infected with a given dose of virus were replaced and viral production was determined by titration on L cells. The detection threshold of the titration was 10^2 PFU/ml. Symbols show multiplicity of infection. (C) Virus production in persistently infected NIH 3T3 cells. A monolayer was infected with 0.1 PFU/cell and maintained as a stationary culture without splitting. Arrows indicate days when incubation medium was replaced with a fresh one.

tion outcome, we compared the expression of virus-encoded proteins and the kinetics of viral RNA accumulation in NIH 3T3 and L cells. First, we infected both cell lines with 10 PFU per cell of MHV-GFP (31) and determined the levels of GFP expression by flow cytometry. Notwithstanding similar kinetics of virus production, at 6 h p.i., only 7% of the NIH 3T3 cells were GFP positive, whereas 60% of L cells expressed GFP (Fig. 2A). At 12 h p.i., when the virus production by the NIH 3T3 cells was higher than that of the L cells at 6 h p.i., only 17% of the GFP-expressing NIH 3T3 cells were detected, which was still 3.5 times lower than in the L cells at 6 h p.i. An accurate flow-cytometry analysis of infected L cells at 12 h p.i. was not possible due to the pronounced cell-cell fusion at that time. Similar results were obtained when NIH 3T3 and L cells were analyzed by fluorescent microscopy for their expression of the viral structural proteins (data not shown). The expression of virus-encoded GFP was not only limited to a smaller fraction of the cell population but was also delayed, as illustrated by a threefold difference in mean GFP fluorescence intensity per NIH 3T3 or L cell at 6 h p.i. (Fig. 2A).

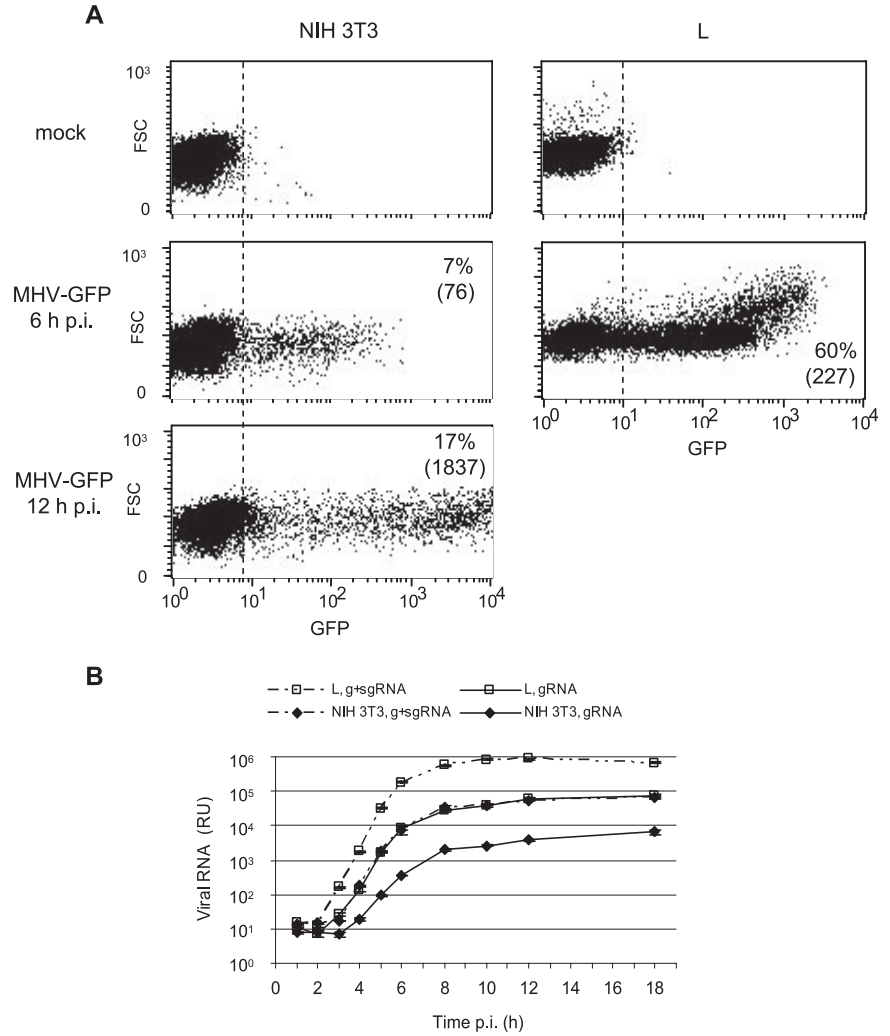

FIG. 2. Virus-encoded proteins and viral RNA in NIH 3T3 and L cells. (A) Percentages and mean fluorescence intensities of GFP-positive cells (in parentheses) are shown within representative dot plots of flow cytometry results. On the *x* axis is GFP fluorescence intensity, and on the *y* axis is forward light scatter (FSC), representative of cell size. (B) Relative amount of viral RNA in 1 ng of total cellular RNA was determined by RT-qPCR and is presented in relative units (RU). qPCR was performed in triplicate. Bars that mostly fit within symbols show standard deviations. NIH 3T3 and L cells were infected with 10 PFU/cell of MHV-GFP (A) or MHV-A59 (B).

Next, we compared the kinetics of viral RNA accumulation in NIH 3T3 and L cells. The cells were infected with 10 PFU per cell, and the relative concentrations of viral RNA were determined by RT-qPCR. The similar amounts of viral RNA associated with the NIH 3T3 and L cells at 1 h p.i. were consistent with the same dose of virus being used to infect the two cell cultures (Fig. 2B). The amplification of gRNA and of g+sgRNA was first detected in the NIH 3T3 cells at 4 h p.i., which was 1 h later than in the L cells. After 3 h p.i., the abundance of both gRNA and g+sgRNA in the NIH 3T3 cells was always at least eight times lower than the respective RNA abundance in the L cells. The largest difference in viral RNA concentrations in the two cell lines, 24-fold for both g+sgRNA and gRNA, was achieved at 6 h p.i. The comparison of the results for the NIH 3T3 cells at 12 h p.i. and for the L cells at 6 h p.i. showed that the former cells contained 3.3-fold and 2.3-fold less g+sgRNA and gRNA, respectively. We conclude that the relatively low abundance of viral RNA templates in the NIH 3T3 cells was likely to be the underlying cause of the reduced expression of viral proteins in these cells.

We investigated whether INT induction was responsible for the limited viral replication in the NIH 3T3 cells. No induction of immediate-early INTα4 or INTβ mRNA was detected in infected NIH 3T3 cells examined by RT-qPCR at every hour between 1 and 6 h p.i. and at 8, 10, 12, 18, and 24 h p.i.

These results showed that NIH 3T3 cells were permissive to MHV and produced high yields of virus. MHV infection caused, however, very limited CPE and cell death in this fibroblastlike cell line. Despite high virus production, the virus genome expression had slower kinetics and was limited to a smaller proportion of the NIH 3T3 culture than in the cells with cytopathic MHV infection. This restriction of infection in NIH 3T3 cells was likely to take effect at the early steps of the viral life cycle, resulting in a decreased accumulation of viral RNA.

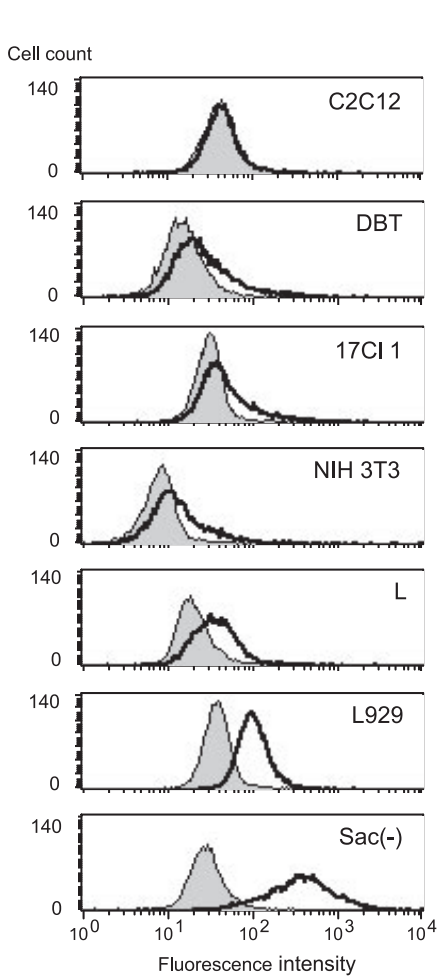

	CEACAM1-positive cells (%)	Relative CEACAM1 density	CPE
C2C12	7 ± 2	2.1 ± 1.1	-
DBT	26 ± 4	4.9 ± 1.3	+
17Cl 1	31 ± 2	3.4 ± 0.1	+
NIH 3T3	43 ± 11	5.9 ± 3.2	-
L	53 ± 7	4.6 ± 2.9	+
L929	78 ± 13	2.7 ± 0.1	+
Sac(-)	97 ± 1	20 ± 4.3	+

FIG. 3. CEACAM1 expression in mouse cell lines. Expression of CEACAM1 on cell surface was determined by staining cells with anti-CEACAM1 monoclonal antibody CC1 and using flow cytometry. Representative histograms are shown. Proportion of CEACAM1-positive cells and relative CEACAM1 density on positive cells were calculated as described in Material and Methods. CPE was registered at 24 h p.i. in cells infected with MHV-A59 (10 PFU/cell).

CEACAM1 expression. The restriction of MHV infection in NIH 3T3 cells could be due to a low abundance of the MHV receptor CEACAM1, which would limit virus entry and spread and CPE development. Therefore, we compared the levels of CEACAM1 expression on the surface of NIH 3T3, L, DBT, 17Cl 1, L929, Sac(-), and C2C12 cell lines. L, DBT, 17Cl 1, L929, and Sac(-) cells are susceptible to a cytopathic, productive MHV infection. C2C12 cells, when infected with a range of virus doses (1 to 100 PFU/cell), produced relatively low virus titers (10^4 to 10^5 PFU/ml) and showed no CPE at 24 h p.i. The cells were stained with fluorescent antibody to CEACAM1 and analyzed by flow cytometry. Except for L929 and Sac(-) cells, the flow cytometry histograms of cells stained for CEACAM1 overlapped considerably with the autofluorescence control histograms (Fig. 3). It made it impossible to discriminate between the possibility that cells in the overlapping part of the histogram were positive, but at low levels, and the possibility that only a fraction of the cells with a fluorescence signal higher than in the control were positive. For comparison, we used a formal procedure of histogram subtraction to get a minimal estimate of CEACAM1 expression and calculated the proportion of cells expressing CEACAM1 and the relative density of the receptor on the cell surface. It is worth noting that the CEACAM1 expression level, in terms of both the percentage of positive cells and the relative receptor density, was not strictly constant (see standard deviation values in Fig. 3). The receptor expression varied from passage to passage or between cells in the same passage but grown with different batches of medium and FCS. The variation in the levels of CEACAM1 expression within the given range did not change the outcome of MHV infection in these cell lines. The lowest number of CEACAM1-positive cells (7%) was found in C2C12 cells. The low level of receptor expression in these cells is likely to contribute to the low viral yields and absence of CPE in these cells. NIH 3T3 cells, with an average of 43% CEACAM1-expressing cells, were within the range of the other cell lines, which develop rapid CPE (26 to 97%). The relative density of the receptor on the surface of receptor-expressing NIH 3T3 cells (average, 5.9) was also within the range of the densities on other cell lines which are killed by MHV (2.7 to 20). The difference in CEACAM1 expression

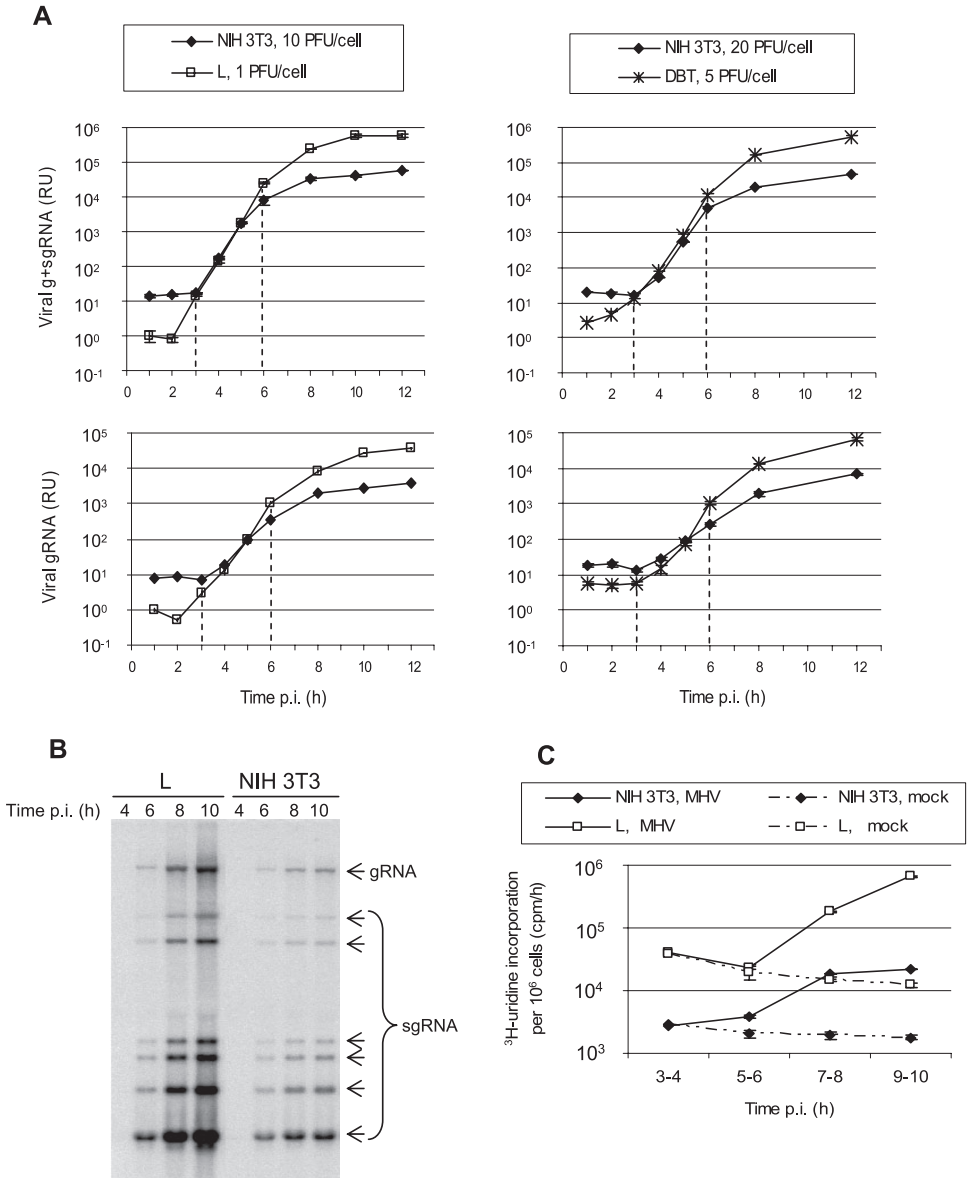

FIG. 4. Viral RNA amplification. Cells were infected with 1 $TCID_{50}$ per cell. (A) The kinetics of viral RNA accumulation, g+sgRNA (two upper graphs) and gRNA (two lower graphs), in NIH 3T3, L, and DBT cells were determined with RT-qPCR as described in the legend for Fig. 2B. Vertical dashed lines encompass the exponential phase of viral RNA amplification. The virus doses, in PFU/cell, are shown above the graphs. (B) Total RNA from infected cells was subjected to gel electrophoresis, and viral RNA was detected by in-gel hybridization. Arrows indicate positions of viral RNA bands. (C) Metabolic labeling of RNA with [^{3}H]uridine in MHV- and mock-infected cells in the presence of actinomycin D. NIH 3T3 and L cells were infected with 10 and 1 PFU/cell, respectively (B and C).

in NIH 3T3 (43%) and L (53%) cells could not explain the approximately 10-fold difference in the percentage of the cells expressing viral proteins (Fig. 2A, 6 h p.i.) and in the viral RNA loads in these cells (Fig. 2B). These results suggest that CEACAM1 is not likely to be the factor limiting MHV infection and CPE in NIH 3T3 cells and that other host factors restrict either virus entry or genome expression in NIH 3T3.

Viral RNA accumulation in NIH 3T3 cells. We next examined whether the accumulation of viral RNA in NIH 3T3 was decreased because viral RNA replication and transcription progressed more slowly in these cells by comparing the rates of viral RNA amplification in NIH 3T3, L, and DBT cells. In these experiments, we infected cells with 1 $TCID_{50}$ per cell using titers that were determined on the respective cell lines. As a result, infection was done with the same functional infectious dose, but, in fact, different numbers of virus particles. L cells needed the least amount of virus to be productively infected. Three- to 5-fold-higher and 10- to 20-fold-higher amounts of virus were required to infect monolayers of DBT and NIH 3T3 cells, respectively. The results of the infectious center assay confirmed that comparable percentages of L (20 to 30%) and NIH 3T3 (8 to 18%) cells were productively infected with 1 $TCID_{50}$ per cell. As in the results of the above-

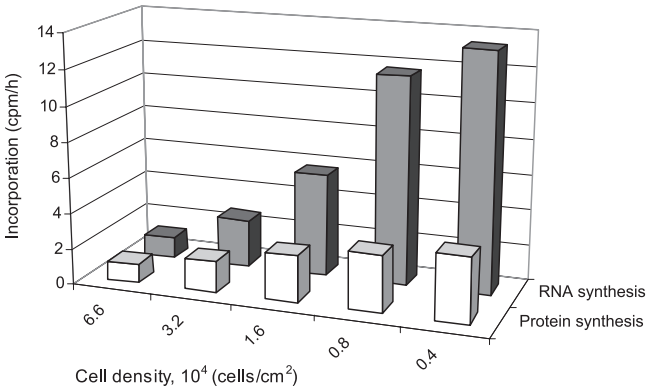

FIG. 5. RNA and protein synthesis in NIH 3T3 cells at different cell densities. RNA and protein synthesis were measured as level of incorporation of [^{3}H]uridine and of [^{35}S]methionine/cysteine, respectively, in 1 h. Incorporation of ^{35}S and ^{3}H was normalized to 1 cell and to 10 cells, respectively, in order to bring values on *y* axis into one range.

described experiment (Fig. 2B), the amounts of viral RNA associated with NIH 3T3, L, and DBT cells at 1 h p.i. were proportional to the input doses of virus (Fig. 4A). Infection with the same functional infectious dose resulted in comparable concentrations of viral RNA in the exponential phase of RNA synthesis, between 3 and 6 h p.i., in the three cell lines. The differential rates of gRNA accumulation in NIH 3T3 and L or DBT cells were suggested by the different slopes of the kinetics graphs in this time interval (Fig. 4A, two lower panels). During this period, one viral genome was amplified to yield 3 to 3.5 genomes in NIH 3T3 cells and 6 and 7 genomes in DBT and L cells, respectively, in 1 h. Thus, the hourly rate of viral genome amplification in NIH 3T3 cells was, on average, two times lower than in L or DBT cells. The rate difference resulted in 8- to 10-fold differences in gRNA accumulation during 3 h. Differently from gRNA amplification, amplification of the g+sgRNA proceeded with a similar rate in NIH 3T3 and L or DBT cells between 3 and 5 h p.i. (Fig. 4A, two upper panels). However, the decline in the rate of g+sgRNA amplification was detected in NIH 3T3 cells 1 h earlier than in L or DBT cells already at 6 h p.i. More-rapid accumulation of viral RNA in L and DBT cells took place before cell-cell fusion could contribute to this process by involving new cells in virus replication. Because of the relatively low cell densities in these experiments, the syncytia included less than 10% of the nuclei of L and DBT cells at 6 h p.i. In-gel hybridization verified that the differences in viral RNA accumulation in NIH 3T3 and L cells applied to all viral RNAs (Fig. 4B). The differences in the rates of viral RNA amplification in NIH 3T3 and L cells were confirmed by metabolic labeling of newly synthesized RNA with [^{3}H]uridine in the presence of actinomycin D. With this method, viral RNA synthesis was not detected at 3 to 4 h p.i. (Fig. 4C). Between 5 and 6 h p.i., the rate of viral RNA synthesis calculated by subtracting [^{3}H]uridine incorporation in mock-infected cells from the value in MHV-infected cells was two times lower in NIH 3T3 cells than in L cells. Later in the infection process, the difference in viral RNA synthesis in NIH 3T3 and L cells increased (10-fold at 7 to 8 h and 32-fold at 9 to 10 h p.i.). At 12 h p.i., the viral RNA loads in NIH 3T3 cells were approximately 1 log lower than in L or DBT cells (Fig. 4A).

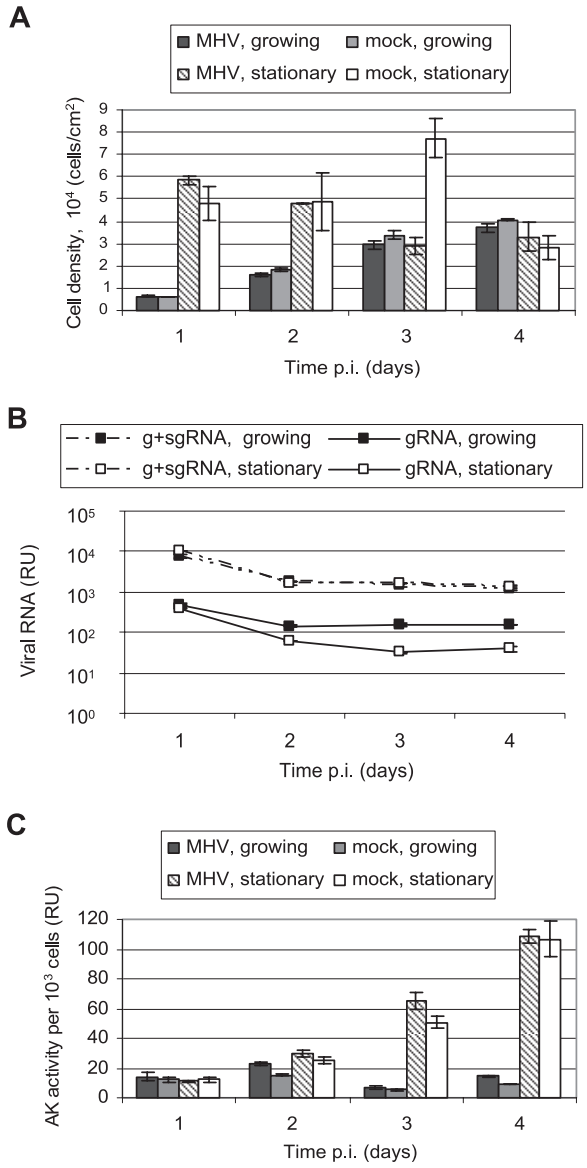

FIG. 6. Cell density, viral RNA, and cell death in growing and stationary cultures of NIH 3T3 cells. Cells in 9-cm^2 dishes were mock or MHV infected (10 PFU/cell). At 4 h p.i., cells in half of the dishes were trypsinized and transferred into dishes with an eightfold-larger surface area. The incubation medium of stationary monolayers was supplemented with 3% FCS, and that of growing monolayers with 8% FCS. At daily intervals, the number of viable cells per dish was counted and cell density was calculated (A), total cellular RNA was isolated for analysis of viral RNA content by RT-qPCR as described in the legend for Fig. 2B (B), and the incubation medium was assayed for activity of AK as a marker of cell death (C). Average values of cell density and AK activity of duplicate dishes are shown. Ranges are indicated in panels A and C.

Altogether, these results showed that the rate of viral RNA accumulation in NIH 3T3 cells was reduced in comparison with the rate in L or DBT cells in which MHV does induce a rapid CPE.

Viral RNA and CPE in growing NIH 3T3 cells. The observation that the residual cellular RNA synthesis in the presence of actinomycin D in mock-infected NIH 3T3 cells was also 1 log lower than in L cells (Fig. 4C) prompted us to investigate whether this difference has any impact on the rate of viral RNA synthesis. We first compared the rates of cellular RNA synthesis in untreated cells. When cells were not treated with actinomycin D, the cellular RNA synthesis was also 10 times slower in NIH 3T3 cells than in L cells (data not shown). The rates of viral RNA synthesis apparently correlated with the rates of cellular RNA synthesis in NIH 3T3 and L cells. We next examined the possibility of increasing cellular RNA synthesis in NIH 3T3 cells by varying the cell densities. The highest cell density tested was similar to the one used for infection experiments, and at this density, the NIH 3T3 cells did not grow further because of contact inhibition. The incorporation of [^{3}H]uridine was much higher in the growing monolayers with low cell densities (Fig. 5). The rate of protein synthesis also increased in growing cells but to a lesser extent. At the smallest and largest cell densities, the rates of RNA and protein synthesis differed by 12- and 3.5-fold, respectively.

Next, we investigated whether MHV infection in growing NIH 3T3 cells with active RNA synthesis would result in a higher accumulation of viral RNA and, possibly, a more-pronounced CPE. We infected NIH 3T3 cells with 10 PFU per cell. Four hours later, cells from half of the dishes were transferred to larger ones, thus removing contact inhibition and providing conditions for cell growth. At daily intervals, we compared cell densities, loads of viral RNA, and the extent of cell death in growing and contact-inhibited, stationary monolayers (Fig. 6A to C). Cells at low density, both MHV- and mock-infected cells, grew at a similar rate till day 3, when the cell growth slowed down because of contact inhibition (Fig. 6A). There was no increase of viral RNA accumulation during the period of cell growth on days 1 and 2 (Fig. 6B). In both growing and stationary cultures, the load of viral RNA diminished between day 1 and 2. The reduction in viral RNA levels could be due to infected-cell death. However, the extent of cell death measured by the activity of AK was similar in all cultures, mock and MHV infected, growing, or stationary, till day 3 (Fig. 6C). The increase in cell death was detected in stationary monolayers, both MHV and mock infected, at days 3 and 4 p.i., possibly because of depletion of growth and attachment factors in the culture medium (42). These results showed that infection of actively dividing NIH 3T3 cells did not result in an increase of viral RNA accumulation or virus-induced cell death, suggesting that the relatively low level of viral RNA in NIH 3T3 cells has another origin than slow synthesis of cellular RNA during contact inhibition.

DISCUSSION

Whether cells will die from a productive viral infection is determined by virus-cell interaction rather than being a property of a virus strain or of particular host cells. The same virus can cause cytopathic and noncytopathic infections in different host cells. On the other hand, both types of infections can occur in the same cells infected with variants of the same virus (9, 17, 47). The cytopathic infection of coronavirus MHV-A59 in established cell lines has been a subject of many studies. Most of the productive, noncytopathic MHV infections described so far have been studied in primary cells or nontransformed cell lines (19, 27, 30). In this report, noncytopathic MHV infection in a 3T3 cell line that was documented earlier (40) was characterized with methods not available 35 years ago in order to identify mechanisms which define the noncytopathic program.

We confirmed earlier observations that MHV infection in NIH 3T3 cells is productive and does not affect the monolayer appearance and density in the acute phase of infection. In the parallel infections, the majority of cells in, for instance, L, DBT, or Sac(-) cultures were killed by MHV within 1 day p.i. Using quantitative assays, we extended the original observation to demonstrate that MHV infection did not accelerate cell death in NIH 3T3 cells in comparison with the rate of cell death in mock-infected control cells up to day 4 p.i. (Fig. 6A, C). Since viral genome expression was found in only a fraction of NIH 3T3 cells in the acute (Fig. 2A) and persistent (O. Slobodskaya, Y. van der Meer, and W. J. M. Spaan, unpublished results) phases of infection, we cannot exclude the possibility that cells expressing viral products die nonsynchronously and undetected. While the fate of individual cells in the infected culture is yet to be elucidated, the survival for up to 1 month of productively infected NIH 3T3 monolayers, visually indistinguishable from uninfected controls, supports the classification of this infection as noncytopathic.

We found that, despite high yields of virus, infection in NIH 3T3 cells was characterized by a relatively low accumulation of viral RNA. Diverse processes involved in the viral life cycle might be rate limiting, resulting in a decreased accumulation of viral RNA. Inefficient entry or postentry steps preceding RNA synthesis will either limit the number of input RNA molecules which initiate replication and transcription or delay the start of RNA synthesis, similarly resulting in a relatively slow RNA accumulation. The possibility that insufficient expression of the MHV receptor CEACAM1 in NIH 3T3 cells was responsible for the restriction of infection was, however, ruled out. A delay in RNA accumulation might also be due to slow viral RNA replication and transcription per se. We found that the rate of viral RNA amplification in the exponential phase of viral RNA synthesis, between 3 and 6 h p.i., was, indeed, reduced in NIH 3T3 cells in comparison with the rate in other cell lines. Mechanistically, a 2-fold difference in hourly rates of gRNA amplification could account for the 10-fold-differential RNA accumulation in cytopathic and noncytopathic infections during the early phase of infection, i.e., the first 3 h. However, since we cannot exclude the possibility that other processes in the early phase of the virus life cycle were also affected in NIH 3T3 cells, the modulation of these processes might also have contributed to the observed differences in viral RNA accumulation.

The absence of a positive correlation of intracellular viral RNA levels and virus yield in NIH 3T3 cells was surprising but has a precedent. Cytopathic and noncytopathic strains of bovine viral diarrhea virus (BVDV), a pestivirus, had up to a 10-fold difference in intracellular virus RNA accumulation although they produced similar virus yields (17). This and our observations suggest that, in productive viral infection in cultured cells, a relatively small fraction of viral products, gRNA and proteins, assembles into viral particles. Host-controlled

processes, e.g., protein maturation, folding, and transport, may be limiting steps in virus production.

The inhibition of viral RNA accumulation of another virus, hepatitis C virus, was found to be associated with the confluent density of Huh-7 monolayers (28, 34). It was shown that smaller intracellular pools of RNA nucleosides in contact-inhibited cultures with low cellular RNA synthesis are responsible for limited synthesis of hepatitis C viral RNA (26). We explored whether a similar mechanism plays a role in the reduced synthesis of coronavirus RNA in contact-inhibited NIH 3T3 cells. Our results showed that the coronavirus RNA synthesis in NIH 3T3 cells is not linked to the level of cellular transcription. The induction of INT response was also ruled out as a mechanism of infection restriction in NIH 3T3.

Relatively slow viral RNA accumulation appears to be a prerequisite for noncytopathic infections. The correlation of decreased cytopathicity and decreased viral RNA amplification was described for a number of RNA-containing viruses, such as the picornavirus hepatitis A virus (47), alphavirus Sindbis virus (9), and pestivirus BVDV (17). Slow kinetics of the accumulation of viral products in the beginning of infection might allow a time frame for the induction of cellular responses which later might control virus replication and the spread of infection between cells and ensure cell survival. The pure dose effect of viral products, however, may not completely explain the development of either cytopathic or noncytopathic programs. The delay of viral RNA accumulation does not necessarily result in the absence of CPE, as demonstrated by the cytopathic infection of some MHV-A59 mutants with delayed RNA synthesis (4, 13). The last observation suggests that relatively dose-independent specific interactions of viral products with cellular counterparts play a role in both viral RNA replication and CPE development. Comparative studies of cytopathic and noncytopathic infections resulted in the identification of the 2BC protein in picornaviruses (47) and the nsp2 protein in Sindbis virus (9) as the viral determinants responsible for efficient viral RNA synthesis and CPE, and this allowed further research into the nature of the cytotoxicity of these viral products (3, 12). In the same way, the study of the intricate regulation of BVDV RNA amplification revealed the role of a host cofactor in the control of the infection outcome (16, 17). The use of NIH 3T3 cells as a host for noncytopathic MHV infection may help in the identification of coronavirus and host factors involved in the regulation of viral RNA synthesis and CPE development.

Most of this study was focused on parameters of viral RNA replication which provided average values for the cell lines. The analysis of viral protein expression on the level of individual cells revealed the heterogeneity of the infected NIH 3T3 cell population despite these cells being genetically uniform. The large amplitude of virus-encoded GFP expression per cell (Fig. 2A, 12 h p.i.) suggests that a hypothetical host factor controlling the replication of viral RNA is expressed unequally within an NIH 3T3 cell population. The heterogeneity of this host factor expression is likely to contribute to MHV persistence in NIH 3T3 cells in a manner similar to the heterogeneous expression of MHV receptor CEACAM1, which was shown to be responsible for MHV persistence in 17Cl 1 and DBT cells (6, 32) by ensuring that only a fraction of the cell population is permissive to efficient virus replication. The pattern of CEACAM1 expression that supported persistent infection in 17Cl 1 and DBT cells was achieved by cytopathic infection-driven selection of the cells. In contrast, the heterogeneous mode of the hypothetical host factor expression in NIH 3T3 is physiological, thus allowing noncytopathic, persistent MHV infection from the beginning.

An interesting finding demonstrated that oncogenic transformation of cells changed the fate of coronavirus infection in these cells from noncytopathic to cytopathic (40). We reproduced this result, having obtained derivative cultures of an NIH 3T3 line which lost contact inhibition and in which MHV infection became cytopathic (O. Slobodskaya and W. J. M. Spaan, unpublished results). If the cytopathicity of coronavirus infection is controlled by a mechanism regulating cell growth, the proposal to use coronaviruses as therapeutic agents in treating tumors will be further substantiated. Enhanced viral replication and CPE in transformed cells targeted by coronavirus, as suggested by Wurdinger et al. (45), by means of an engineered tumor-specific receptor affinity might ensure effective killing of these cells. The knowledge of the mechanisms of host-specific control of coronavirus RNA synthesis, on one hand, and virus impact on host cells, on the other hand, could advance our understanding of virus tissue tropism and infection pathogenesis.

ACKNOWLEDGMENTS

We are grateful to Kathryn Holmes and Susan Weiss for providing anti-CEACAM1 CC1 monoclonal antibody and MHV-GFP virus, respectively. We thank Peter Bredenbeek for critical reading of the manuscript and Eric Snijder for helpful suggestions.

REFERENCES

1. **Arbour, N., G. Cote, C. Lachance, M. Tardieu, N. R. Cashman, and P. J. Talbot.** 1999. Acute and persistent infection of human neural cell lines by human coronavirus OC43. J. Virol. **73:**3338–3350.
2. **Arbour, N., S. Ekande, G. Cote, C. Lachance, F. Chagnon, M. Tardieu, N. R. Cashman, and P. J. Talbot.** 1999. Persistent infection of human oligodendrocytic and neuroglial cell lines by human coronavirus 229E. J. Virol. **73:**3326–3337.
3. **Barco, A., and L. Carrasco.** 1998. Identification of regions of poliovirus 2BC protein that are involved in cytotoxicity. J. Virol. **72:**3560–3570.
4. **Brockway, S. M., and M. R. Denison.** 2005. Mutagenesis of the murine hepatitis virus nsp1-coding region identifies residues important for protein processing, viral RNA synthesis, and viral replication. Virology **340:**209–223.
5. **Chan, P. K., K. F. To, A. W. Lo, J. L. Cheung, I. Chu, F. W. Au, J. H. Tong, J. S. Tam, J. J. Sung, and H. K. Ng.** 2004. Persistent infection of SARS coronavirus in colonic cells in vitro. J. Med. Virol. **74:**1–7.
6. **Chen, W., and R. S. Baric.** 1996. Molecular anatomy of mouse hepatitis virus persistence: coevolution of increased host cell resistance and virus virulence. J. Virol. **70:**3947–3960.
7. **Choi, K. S., P. Huang, and M. M. Lai.** 2002. Polypyrimidine-tract-binding protein affects transcription but not translation of mouse hepatitis virus RNA. Virology **303:**58–68.
8. **Choi, K. S., A. Mizutani, and M. M. Lai.** 2004. SYNCRIP, a member of the heterogeneous nuclear ribonucleoprotein family, is involved in mouse hepatitis virus RNA synthesis. J. Virol. **78:**13153–13162.
9. **Dryga, S. A., O. A. Dryga, and S. Schlesinger.** 1997. Identification of mutations in a Sindbis virus variant able to establish persistent infection in BHK cells: the importance of a mutation in the nsP2 gene. Virology **228:**74–83.
10. **Dveksler, G. S., M. N. Pensiero, C. B. Cardellichio, R. K. Williams, G. S. Jiang, K. V. Holmes, and C. W. Dieffenbach.** 1991. Cloning of the mouse hepatitis virus (MHV) receptor: expression in human and hamster cell lines confers susceptibility to MHV. J. Virol. **65:**6881–6891.
11. **Enjuanes, L., F. Almazan, I. Sola, and S. Zuniga.** 2006. Biochemical aspects of coronavirus replication and virus-host interaction. Annu. Rev. Microbiol. **60:**211–230.
12. **Garmashova, N., R. Gorchakov, E. Frolova, and I. Frolov.** 2006. Sindbis virus nonstructural protein nsP2 is cytotoxic and inhibits cellular transcription. J. Virol. **80:**5686–5696.
13. **Graham, R. L., and M. R. Denison.** 2006. Replication of murine hepatitis virus is regulated by papain-like proteinase 1 processing of nonstructural proteins 1, 2, and 3. J. Virol. **80:**11610–11620.

14. **Hilton, A., L. Mizzen, G. MacIntyre, S. Cheley, and R. Anderson.** 1986. Translational control in murine hepatitis virus infection. J. Gen. Virol. **67:** 923–932.
15. **Huang, P., and M. M. Lai.** 1999. Polypyrimidine tract-binding protein binds to the complementary strand of the mouse hepatitis virus 3′ untranslated region, thereby altering RNA conformation. J. Virol. **73:**9110–9116.
16. **Lackner, T., A. Muller, M. Konig, H. J. Thiel, and N. Tautz.** 2005. Persistence of bovine viral diarrhea virus is determined by a cellular cofactor of a viral autoprotease. J. Virol. **79:**9746–9755.
17. **Lackner, T., A. Muller, A. Pankraz, P. Becher, H. J. Thiel, A. E. Gorbalenya, and N. Tautz.** 2004. Temporal modulation of an autoprotease is crucial for replication and pathogenicity of an RNA virus. J. Virol. **78:**10765–10775.
18. **Lai, M. M.** 1998. Cellular factors in the transcription and replication of viral RNA genomes: a parallel to DNA-dependent RNA transcription. Virology **244:**1–12.
19. **Lavi, E., A. Suzumura, M. Hirayama, M. K. Highkin, D. M. Dambach, D. H. Silberberg, and S. R. Weiss.** 1987. Coronavirus mouse hepatitis virus (MHV)-A59 causes a persistent, productive infection in primary glial cell cultures. Microb. Pathog. **3:**79–86.
20. **Lavi, E., Q. Wang, S. R. Weiss, and N. K. Gonatas.** 1996. Syncytia formation induced by coronavirus infection is associated with fragmentation and rearrangement of the Golgi apparatus. Virology **221:**325–334.
21. **Leibowitz, J. L., C. W. Bond, K. Anderson, and S. Goss.** 1984. Biological and macromolecular properties of murine cells persistently infected with MHV-JHM. Arch. Virol. **80:**315–332.
22. **Li, H. P., X. Zhang, R. Duncan, L. Comai, and M. M. Lai.** 1997. Heterogeneous nuclear ribonucleoprotein A1 binds to the transcription-regulatory region of mouse hepatitis virus RNA. Proc. Natl. Acad. Sci. USA **94:**9544–9549.
23. **Li, W., T. C. Greenough, M. J. Moore, N. Vasilieva, M. Somasundaran, J. L. Sullivan, M. Farzan, and H. Choe.** 2004. Efficient replication of severe acute respiratory syndrome coronavirus in mouse cells is limited by murine angiotensin-converting enzyme 2. J. Virol. **78:**11429–11433.
24. **Mizzen, L., S. Cheley, M. Rao, R. Wolf, and R. Anderson.** 1983. Fusion resistance and decreased infectability as major host cell determinants of coronavirus persistence. Virology **128:**407–417.
25. **Nanda, S. K., and J. L. Leibowitz.** 2001. Mitochondrial aconitase binds to the 3′ untranslated region of the mouse hepatitis virus genome. J. Virol. **75:** 3352–3362.
26. **Nelson, H. B., and H. Tang.** 2006. Effect of cell growth on hepatitis C virus (HCV) replication and a mechanism of cell confluence-based inhibition of HCV RNA and protein expression. J. Virol. **80:**1181–1190.
27. **Okumura, A., K. Machii, S. Azuma, Y. Toyoda, and S. Kyuwa.** 1996. Maintenance of pluripotency in mouse embryonic stem cells persistently infected with murine coronavirus. J. Virol. **70:**4146–4149.
28. **Pietschmann, T., V. Lohmann, G. Rutter, K. Kurpanek, and R. Bartenschlager.** 2001. Characterization of cell lines carrying self-replicating hepatitis C virus RNAs. J. Virol. **75:**1252–1264.
29. **Rao, P. V., and T. M. Gallagher.** 1998. Intracellular complexes of viral spike and cellular receptor accumulate during cytopathic murine coronavirus infections. J. Virol. **72:**3278–3288.
29a. **Reed, L. J., and H. Muench.** 1938. A simple method of estimating fifty percent end point. Am. J. Hyg. **27:**493–497.
30. **Rempel, J. D., L. A. Quina, P. K. Blakely-Gonzales, M. J. Buchmeier, and D. L. Gruol.** 2005. Viral induction of central nervous system innate immune responses. J. Virol. **79:**4369–4381.
31. **Sarma, J. D., E. Scheen, S. H. Seo, M. Koval, and S. R. Weiss.** 2002. Enhanced green fluorescent protein expression may be used to monitor murine coronavirus spread in vitro and in the mouse central nervous system. J. Neurovirol. **8:**381–391.
32. **Sawicki, S. G., J. H. Lu, and K. V. Holmes.** 1995. Persistent infection of cultured cells with mouse hepatitis virus (MHV) results from the epigenetic expression of the MHV receptor. J. Virol. **69:**5535–5543.
33. **Sawicki, S. G., D. L. Sawicki, and S. G. Siddell.** 2007. A contemporary view of coronavirus transcription. J. Virol. **81:**20–29.
34. **Scholle, F., K. Li, F. Bodola, M. Ikeda, B. A. Luxon, and S. M. Lemon.** 2004. Virus-host cell interactions during hepatitis C virus RNA replication: impact of polyprotein expression on the cellular transcriptome and cell cycle association with viral RNA synthesis. J. Virol. **78:**1513–1524.
35. **Shi, S. T., P. Huang, H. P. Li, and M. M. Lai.** 2000. Heterogeneous nuclear ribonucleoprotein A1 regulates RNA synthesis of a cytoplasmic virus. EMBO J. **19:**4701–4711.
36. **Shi, S. T., J. J. Schiller, A. Kanjanahaluethai, S. C. Baker, J. W. Oh, and M. M. Lai.** 1999. Colocalization and membrane association of murine hepatitis virus gene 1 products and de novo-synthesized viral RNA in infected cells. J. Virol. **73:**5957–5969.
37. **Siddell, S., H. Wege, A. Barthel, and V. ter Meulen.** 1981. Coronavirus JHM: intracellular protein synthesis. J. Gen. Virol. **53:**145–155.
38. **Spaan, W. J., P. J. Rottier, M. C. Horzinek, and B. A. van der Zeijst.** 1981. Isolation and identification of virus-specific mRNAs in cells infected with mouse hepatitis virus (MHV-A59). Virology **108:**424–434.
39. **Spagnolo, J. F., and B. G. Hogue.** 2000. Host protein interactions with the 3′ end of bovine coronavirus RNA and the requirement of the poly(A) tail for coronavirus defective genome replication. J. Virol. **74:**5053–5065.
40. **Sturman, L. S., and K. K. Takemoto.** 1972. Enhanced growth of a murine coronavirus in transformed mouse cells. Infect. Immun. **6:**501–507.
41. **Todaro, G. J., and H. Green.** 1963. Quantitative studies of the growth of mouse embryo cells in culture and their development into established lines. J. Cell Biol. **17:**299–313.
42. **Todaro, G. J., G. K. Lazar, and H. Green.** 1965. The initiation of cell division in a contact-inhibited mammalian cell line. J. Cell. Physiol. **66:**325–333.
43. **Tresnan, D. B., R. Levis, and K. V. Holmes.** 1996. Feline aminopeptidase N serves as a receptor for feline, canine, porcine, and human coronaviruses in serogroup I. J. Virol. **70:**8669–8674.
44. **Versteeg, G. A., O. Slobodskaya, and W. J. Spaan.** 2006. Transcriptional profiling of acute cytopathic murine hepatitis virus infection in fibroblast-like cells. J. Gen. Virol. **87:**1961–1975.
45. **Wurdinger, T., M. H. Verheije, M. Raaben, B. J. Bosch, C. A. de Haan, V. W. van Beusechem, P. J. Rottier, and W. R. Gerritsen.** 2005. Targeting non-human coronaviruses to human cancer cells using a bispecific single-chain antibody. Gene Ther. **12:**1394–1404.
46. **Yu, G. Y., and M. M. Lai.** 2005. The ubiquitin-proteasome system facilitates the transfer of murine coronavirus from endosome to cytoplasm during virus entry. J. Virol. **79:**644–648.
47. **Zhang, H., S. F. Chao, L. H. Ping, K. Grace, B. Clarke, and S. M. Lemon.** 1995. An infectious cDNA clone of a cytopathic hepatitis A virus: genomic regions associated with rapid replication and cytopathic effect. Virology **212:**686–697.
48. **Zhou, H., and S. Perlman.** 2006. Preferential infection of mature dendritic cells by mouse hepatitis virus strain JHM. J. Virol. **80:**2506–2514.